FLORIDA STATE UNIVERSITY

COLLEGE OF ARTS AND SCIENCES

A SEARCH FOR QUANTUM BLACK HOLE PRODUCTION IN PROTON-PROTON COLLISIONS AT $\sqrt{S}$= 13 TEV REQUIRING TWO HIGH ENERGY PHOTONS

By

STEVEN W. TOLBERT

A Thesis submitted to the
Department of Physics
in partial fulfillment of the
requirements for the degree of
Bachelor of Science

2017

Steven W. Tolbert defended this thesis on April 21, 2017.
The members of the supervisory committee were:

Dr. Andrew Askew
Thesis Director

Dr. Todd Adams
Committee Member

Dr. Mark Sussman
Committee Member

ACKNOWLEDGMENTS

I would like to thank my family for all they have done for me to get me to this point. My father who has always pushed me to work harder and explore further, my mother who believes in my dreams and aspirations, and my siblings who have always been there for me. Without any of you, none of this would have been possible.

I would like to also thank Dr. Andrew Askew, who guided me through this thesis with his extraordinary knowledge of physics, and who has mentored me since I arrived at Florida State. I am forever grateful for the time and expertise he has shared with me throughout the years.

TABLE OF CONTENTS

List of Tables . . . v
List of Figures . . . vi
Abstract . . . viii

1 Introduction and Motivation **1**

2 Theory **2**
2.0.1 CATFISH . . . 2
2.0.2 Jet Clustering . . . 3
2.0.3 Candidate Events . . . 4
2.0.4 Monte Carlo ST Distributions . . . 6

3 Primer to Analysis **9**
3.0.1 Jets . . . 9
3.0.2 Momentum in the Transverse Direction : P_T . . . 9

4 The CMS Experiment **10**
4.0.1 Tracker . . . 11
4.0.2 ECAL . . . 11
4.0.3 HCAL . . . 11
4.0.4 CMS Magnet . . . 12
4.0.5 Muon Detectors . . . 12
4.0.6 Triggers . . . 12
4.0.7 Smearing . . . 13

5 Data **19**
5.0.1 LHC Data Information . . . 19
5.0.2 Method of Analysis . . . 19

6 Selection **20**
6.0.1 Photon Multiplicity Cut . . . 20
6.0.2 Calorimeter Region Selection Cuts . . . 21
6.0.3 Photon Identification Cuts . . . 22

7 Analysis **25**
7.0.1 Functional Form . . . 26
7.0.2 Control Region Fit on Signal Region . . . 28

8 Results **33**

Bibliography . . . 34

LIST OF TABLES

2.1 CATFISH Parameters 3

2.2 Candidate Events With Various Requirements 5

6.1 Isolation Requirements 24

7.1 P_N Values for Two Good Photons 26

7.2 P_N Values for One Good and 1 Bad Photon 27

7.3 Integral of $f_j(x)$ from 1500 to 2400 for 2 Good Photons 30

7.4 Integral of $f_j(x)$ from 1500 to 2400 for 1 Good 1 Bad Photon 32

LIST OF FIGURES

2.1 Number of Jets Per Event from CATFISH 4

2.2 Number of Photons Per Event from CATFISH 5

2.3 Ideal S_T Distribution from CATFISH 6

2.4 Vector Imbalance S_T Distribution from CATFISH 7

2.5 Non-Smeared Ideal and Vector S_T Distribution from CATFISH 8

4.1 The CMS Detector [5] 10

4.2 Ideal S_T Distribution from CATFISH Smeared to CMS Resolution 13

4.3 Ideal S_T Versus Smeared Ideal S_T 14

4.4 Vector Imbalance S_T Distribution from CATFISH Smeared to CMS Resolution 15

4.5 Vector Imbalance S_T versus Smeared Vector Imbalance S_T 15

4.6 Smeared Photon P_T Versus Non-Smeared Photon P_T 16

4.7 Smeared Pion P_T Versus Non-Smeared Pion P_T 16

4.8 Smeared Vector ST for Events With Zero High Energy Photons 17

4.9 Smeared Vector S_T for Two+ Photon Events 17

6.1 Leading Photon PT 20

6.2 Trailing Photon PT 21

6.3 Photon Eta 22

6.4 Photon Phi 22

6.5 $\sigma_{i\eta i\eta}$ Distribution 23

7.1 0+ Jet S_T For Two Good Photons 25

7.2 Integral Normalized $f(x)$ For 2 Good Photons and Varied Jet Multiplicity 27

7.3 Integral Normalized $f(x)$ For 1 Good Photon 1 Bad Photon and Varied Jet Multiplicity 28

7.4 0,1,2 Jets $f(x)$ For 2 Good Photons Scaled to 3+ Jet S_T 29

7.5 0,1,2 Jets $f(x)$ For 2 Good Photons Scaled to 3+ Jet Signal Region S_T 30

7.6 0,1,2 Jets $f(x)$ For 1 Good Photon 1 Bad Photon Scaled to 3+ Jet S_T 31
7.7 0 Jet $f(x)$ For 1 Good Photon 1 Bad Photon Scaled to 3+ Jet Signal Region S_T . . . 32

ABSTRACT

This thesis searches for new physics at CMS in the form of microscopic black hole production at a minimum threshold of formation of 2.0 TeV. This analysis will examine data from Run II of the LHC with center-of-mass energy $\sqrt{s}$=13 TeV, and an integrated luminosity of 12.9 ± 0.8 fb^{-1}. This is the first analysis to search for microscopic black hole production with the requirement of two high P_T photons in the final state. After modeling backgrounds through low jet multiplicity control regions, no statistically significant excess is found in the signal region.

CHAPTER 1

INTRODUCTION AND MOTIVATION

There exist four fundamental forces in the universe that we are aware of. These forces listed in order of strength are: the strong force, the electro-magnetic force, the weak force, and the gravitational force. The Hierarchy Problem [3] states that there is a large discrepancy between the weak and gravitational fundamental forces where the difference in strength between these forces is extraordinarily large. This raises questions regarding the nature of these forces and our current description of the universe. A solution proposed by Nima Arkani-Hamad, Savas Dimopolos and Gia Dvali known as the "ADD model" invokes large extra dimensions to unite the "gravitational and gauge interactions at the weak scale." [3] By this process, the ADD model allows for the large discrepancy between the weak and gravitational forces to vanish because there was no large discrepancy to begin with; rather, gravitational experiments are measuring a form of gravity that is diluted due to these large extra dimensions. Such a solution to the hierarchy problem would provide several testable predictions that manifest themselves in the physical world making it a viable theory to explore.

Of particular interest to this analysis, the ADD model lowers the Planck Mass (M_{pl}), which is the minimum mass required for a black hole to form, into energies obtainable at the LHC. When extra dimensions are incorporated, one finds that the value of the Planck mass changes with the number of dimensions, n, as well as the size of said dimensions, R. Mathematically this is defined as:

$$M_D^{n+2} = \frac{M_{pl}^2}{8\pi R^n} \tag{1.1}$$

Where M_D is the n-dimensional Planck mass, and M_{pl} is the current value of the Planck mass.

Current models of superstring theory depend on three spatial dimensions, 1 time dimension, and 6 compact spatial dimensions (3+1+6) [12]. This analysis will search for microscopic black holes under the model for superstring theory. However, this analysis can easily be adapted for different flavors of string theory or other models that contain any number of extra spatial dimensions.

CHAPTER 2

THEORY

Microscopic black holes will decay in four distinct phases, as described in detail by Bleicher, Nicolini, and Sprenger [6]:

- Balding Phase: When the black hole forms, it will be a highly asymmetric object with gauge field hair. In the initial stage of the evolution, the black hole hair is shed (mainly by the Schwinger pair production mechanism) and asymmetries are lost via gravitational radiation.
- Spin-Down Phase: At the end of the balding phase, the highly spinning, neutral black hole loses mass and angular momentum through Hawking and Unruh-Starobinskii radiation.
- Schwarzschild Phase: At the end of the spin-down phase, the resulting spherically symmetric black hole continues to evaporate but now in a spherical manner. This results in the gradual decrease of its mass and the increase of its temperature.
- Planck Phase: When the mass and/or the Hawking temperature approaches the fundamental scale $T \sim M \sim M*$, the black hole can no be longer described semi-classically. A theory of quantum gravity is necessary to study this phase in detail.

Phases that are relevant to this analysis are the Spin-Down and Schwarzschild phases where Hawking radiation takes place. During phases in which Hawking radiation takes place our black hole will decay into all standard model (SM) particles until it reaches the Planck mass. Once this occurs the black hole will be classified as a Quantum Black Hole (QBH) and requires a quantum theory of gravity to analyze further.

2.0.1 CATFISH

In order to simulate events in which Black Holes are produced this analysis will use the Monte Carlo generator CATFISH: Collider grAviTational FIeld Simulator for black Holes. [8] Other generators include BlackMax and CHARYBDIS each having their own advantages and disadvantages [11]. CATFISH allows for the modeling of gravitational loss from gravitons escaping into large extra dimensions providing a more complete simulation of black hole decay in accordance with current theoretical models. Under the given parameters, CATFISH will generate events in which black holes are created under the Yoshino-Rychkov gravitational loss model with electromagnetic charge conservation.

Using CATFISH this analysis will be able to examine events in which black holes are produced to create a benchmark of values to compare to data obtained during run II at the LHC. A full account of generator parameters are listed in Table 2.1

Table 2.1: CATFISH Parameters

Parameter	Value
Fundamental Scale	1.0 TeV
Minimum Mass at Formation	2.0 TeV
Minimum Mass Threshold at Evaportaion	1.0 TeV
Number of Final Quanta	2
Number of Extra Dimensions	6
Number of Events	100000
EM Charge Conservation	Yes
Gravitational Loss Model	Yoshino-Rychkov

The quantities of interest this analysis wishes to extract from the generator include:

- The scalar sum of transverse momenta which will further be defined as S_T.
- How many photons are in each event.
- How many jets are in each event.
- The number of candidate events.
- How the number of candidate events scale with jet multiplicity.

2.0.2 Jet Clustering

CATFISH clusters jets based on PYTHIAs PYCELL jet clustering algorithm which defaults the P_T requirement of a jet to 7 GeV [13]. For this analysis, the jets are required to have $P_T > 40$ GeV and as such jets need to be clustered outside of CATFISH as there is no easy way to change the P_T requirement on the jets within the generator.

For this objective, Jets are clustered using the FastJet [7] package with a distance parameter of R=0.4 using the anti-k_t algorithm. The anti-k_t algorithm is chosen for its ability to resolve jets efficiently. This algorithm and distance parameter is also chosen for its use in previous CMS studies. [1]

Requiring that the jets have $P_T > 40$ GeV yields the following jet distribution shown in Figure 2.1.

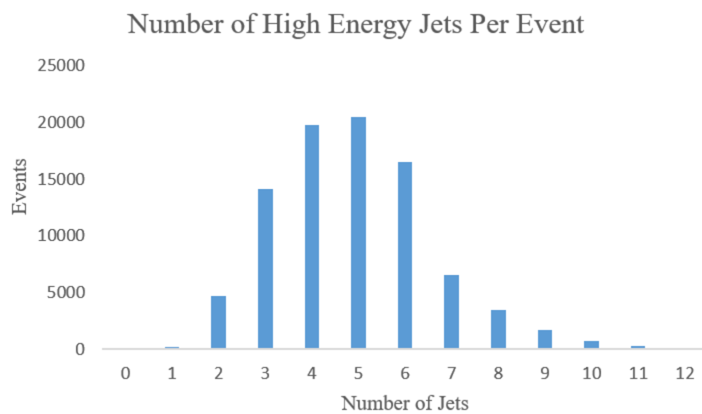

Figure 2.1: Number of Jets Per Event from CATFISH

One can see that most events in which black hole production takes place will have a significant number of jets; likewise, events with low jet multiplicity are unlikely to contain black hole production. This will become key in defining the background when analyzing data.

2.0.3 Candidate Events

At the generator level a candidate event is defined as an event which contains two photons whose P_T are above 40 GeV. When analyzing data collected at the LHC, the definition of a candidate event will become more strict.

Figure 2.2 displays the number of events containing N number of photons. For this analysis, the requirement of two high E_T photons was chosen to gain access to the diphoton trigger. From Fig. 2.2 this choice is justified as there is a significant number of events that contain at two or more photons.

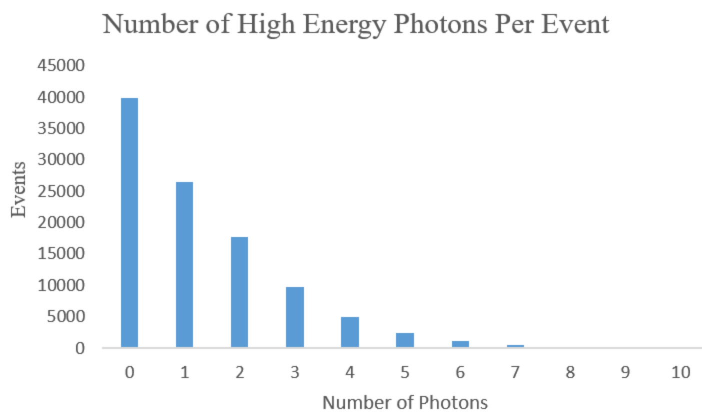

Figure 2.2: Number of Photons Per Event from CATFISH

This analysis then must consider how the number of candidate events at the generator level scales with jet multiplicity. This is shown in Table 2.2.

Table 2.2: Candidate Events With Various Requirements

Requirement	Number of Candidates
Two Photons	100000
Two Photons with $P_T > 40$ GeV	36291
Two Photons with $P_T > 40$ GeV and 0+ Jets	36291
Two Photons with $P_T > 40$ GeV and 1+ Jets	36291
Two Photons with $P_T > 40$ GeV and 2+ Jets	36291
Two Photons with $P_T > 40$ GeV and 3+ Jets	36287

One can see that approximately 36% of the events produced in quantum black hole production will result in two or more high P_T photons. This a sizable fraction of our events and thus ensures that this analysis is viable.

The S_T is the next quantity of interest from the generator. This analysis will use the S_T distribution to search for black hole production for the following reasons [1]:

- S_T is not sensitive to the abundance of particles produced in black hole decay.
- The shape of S_T distribution is independent of object multiplicity for QCD.
- S_T is directly related to the energy of collision.

This makes S_T a robust quantity for searching for new physics and will be a key part to this analysis.

Previous studies at the LHC have shown that the background will be dominated by QCD multi-jet production which will produce a decaying exponential S_T distribution [1]; however, if one encounters black hole production, some structure will begin to form past a certain threshold that is not indicative of QCD.

2.0.4 Monte Carlo ST Distributions

For the purposes of this analysis the S_T distribution will be defined as the scalar sum of momentum in the transverse direction of photons, leptons, anti-leptons, jets and MET. This is mathematically defined:

$$S_{T,Ideal} = \sum_{i}^{vis} P_{T,i} + \sum_{i}^{invis} P_{T,i} \tag{2.1}$$

Calculating the S_T in this manner produces the following S_T distribution seen in Figure 2.3:

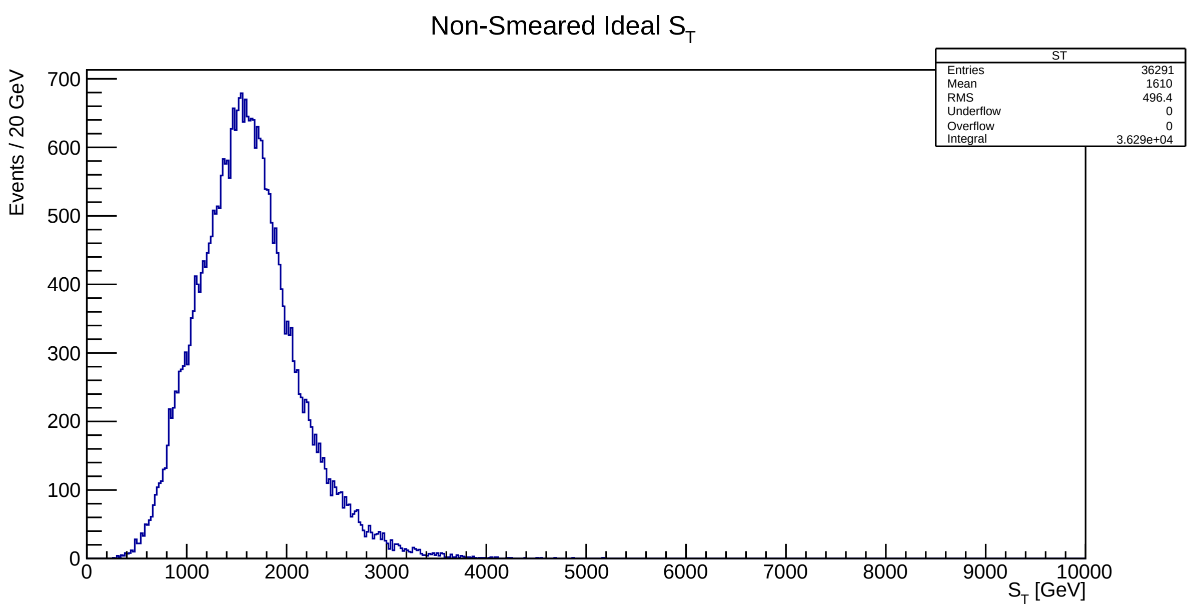

Figure 2.3: Ideal S_T Distribution from CATFISH

The ideal S_T produced at the generator level is far too idealized for real analysis as the generator provides information not available to the detector such as the momentum of particles who are not able to measured. These particles include gravitons which would be produced in quantum black hole decay and particles who will rarely interact with the detector such as neutrinos. In order to create a S_T distribution that does not use this information, one can define the S_T as a vector imbalance defined as:

$$S_{T,Vector} = \sum_{i}^{vis} P_{T,i} + |\sum_{i}^{vis} \vec{P}_{T,i}| \tag{2.2}$$

Calculating the S_T in this manner allows the generator to create an S_T distribution without using the momentum of invisible particles. Doing this produces the following S_T distribution Figure 2.4.

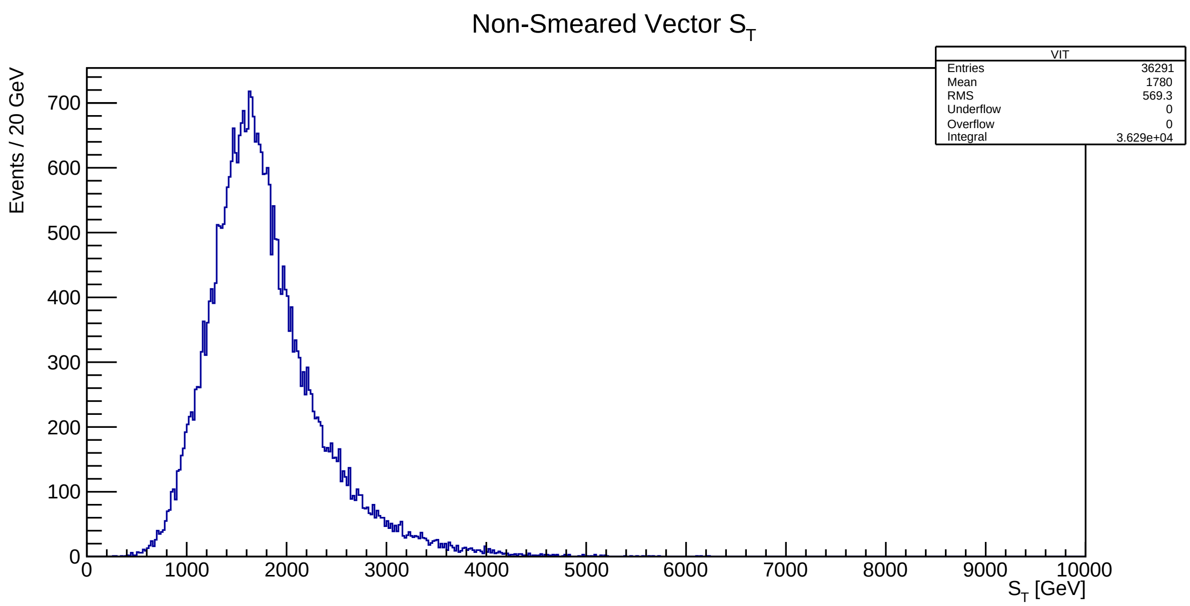

Figure 2.4: Vector Imbalance S_T Distribution from CATFISH

To better compare these two S_T distributions the overlay of the two is shown in Figure 2.5 with the ideal S_T displayed in blue and the vector S_T displayed in red. This plot shows that when calculating the S_T using the vector imbalance method, the S_T is shifted into a slightly higher S_T region.

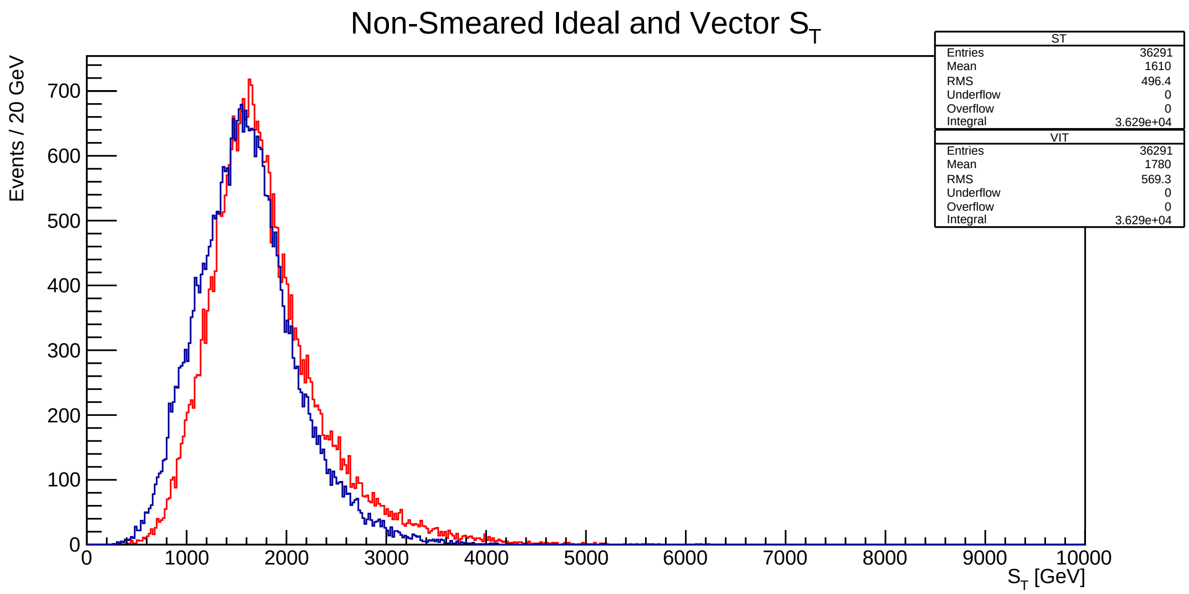

Figure 2.5: Non-Smeared Ideal and Vector S_T Distribution from CATFISH

From these plots one can see that in the case of quantum black hole production with a minimum mass threshold of formation at 2.0 TeV, the S_T distribution does not result in a narrow peak at 2.0 TeV; rather, a broad distribution is formed near the minimum mass of formation. However, when this same distribution is measured at CMS, one must account for the resolution of the measurements. This process is known as smearing and will be discussed in further detail in subsequent sections.

CHAPTER 3

PRIMER TO ANALYSIS

3.0.1 Jets

In a proton-proton collision one is colliding the partons that compose the proton (gluons, two up-quarks and a down-quark), which cannot exist in an isolated state due to color confinement. Rather than separating after a collision, the quarks will transfer energy into mass and produce quark antiquark pairs. This process results in the creation of hadronic jets which manifest themselves in the detector and can be measured and analyzed.

3.0.2 Momentum in the Transverse Direction : P_T

The momentum in the direction transverse to the beam pipe is defined as:

$$P_T^2 = P_X^2 + P_Y^2 \tag{3.1}$$

The basis for nearly all of physics are conservation laws. Before the collision the momentum in the transverse direction P_T is equal to zero, after the collision of two protons (or more accurately the partons within them), all momentum in the transverse direction is the result of particle collisions. The P_T should thus be balanced so that the vector sum of P_T is equal to zero; however, this is not the case. For example: weakly interacting particles such as neutrinos will rarely interact with the detector. The remaining P_T required to balance the measured P_T is known as the missing transverse energy (MET). The MET is due to particles that are not able to be measured by the detector, this includes neutrinos and hypothetical particles such as gravitons that would be produced by microscopic black holes.

CHAPTER 4

THE CMS EXPERIMENT

The Compact Muon Solenoid (CMS) detector is a large particle detector built along the LHC at CERN. The CMS detector uses a 4 T magnetic field to curve the motion of charged particles produced in proton-proton collisions at the LHC. The CMS detector is composed of five layers: Tracker, Electromagnetic Calorimeter, Hadronic Calorimeter, Magnet, and the Muon Detectors. To increase the longevity of the magnet, the CMS magnet is run with a 3.8 Tesla magnetic field instead of its full strength of 4 Tesla. [9]

A cross-sectional view of the detector is shown in Fig. 4.1

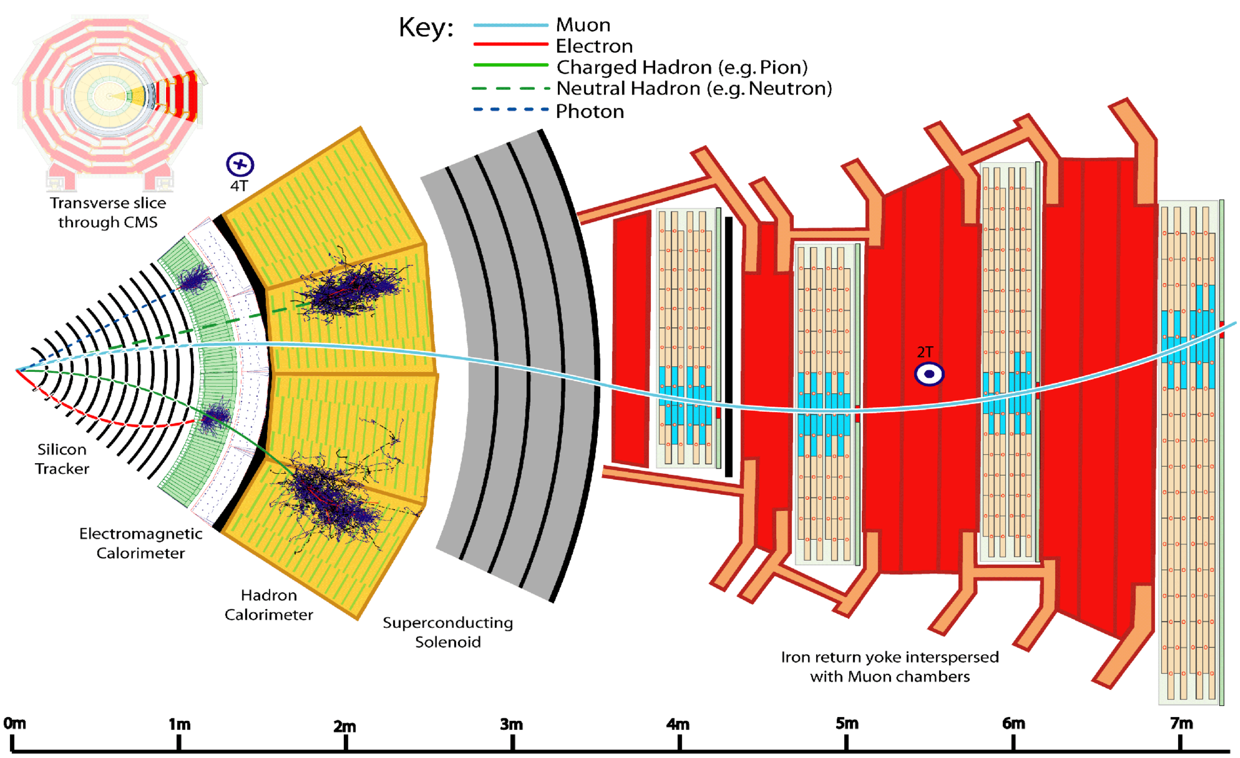

Figure 4.1: The CMS Detector [5]

4.0.1 Tracker

The CMS tracker is composed entirely of silicon and tracks the path of particles resulting from collisions by measuring the position of particles along a few key points within an accuracy of 10 μm. This allows for the measurement of curvature that particle's path has in the magnetic field, and from this one can derive the momentum of the particle.

4.0.2 ECAL

After the particle travels out of the tracker it traverses the electromagnetic calorimeter (ECAL). The ECAL is a homogeneous crystal calorimeter composed of a barrel section (EB) spanning $|\eta| \leq 1.4$ and two endcaps (EE) spanning $1.6 \leq \eta \leq 2.4$. The ECAL is composed of 75,848 $PbWO_4$ crystals having a radiation length of X_0=0.89 cm and are divided into supermodules containing 1700 crystals each in the barrel. Lead tungstate crystals were chosen for its high density, short radiation length of .89 cm and small Moliere radius of 2.19 cm. The ECAL will measure electromagnetic objects such as photons and electrons by measuring the scintillation light produced from interactions within the crystals through avalanche photodiodes.
The CMS ECAL has an energy resolution of [9]

$$\frac{\sigma_E}{E} = \frac{2.8\%\sqrt{GeV}}{\sqrt{E(GeV)}} \oplus \frac{12\%GeV}{E(GeV)} \oplus 0.3\%. \tag{4.1}$$

The energy resolution shown above is a quadratic sum, which is defined as:

$$A \oplus B = \sqrt{A^2 + B^2}. \tag{4.2}$$

For the ECAL energy resolution: the first term added in quadrature represents the the stochastic term and accounts for the variability of objects that will generate a signal in the detector. The second term accounts for the noise generated from electronics and the final term represents a constant that accounts for any physical design constraints and calibration of the CMS detector. For high energy objects, such as the photons being required in this analysis, the constant term in the ECAL resolution becomes the dominant term in defining the resolution.

4.0.3 HCAL

Hadrons will continue on through the electromagnetic calorimeter and deposit energy into the hadronic calorimeter (HCAL). The hadronic calorimeter is a hermetic sampling calorimeter comprised of brass and steel absorbing material and plastic scintillators. When a hadron hits an absorber it will cascade into secondary particles producing scintillation light that can be read out by the hybrid photodiodes. The resolution of the ECAL + HCAL is found to be [9]:

$$\frac{\sigma_E}{E} = \frac{111\%\sqrt{GeV}}{\sqrt{E(GeV)}} \oplus 8.6\% \tag{4.3}$$

4.0.4 CMS Magnet

Just beyond the HCAL lies the CMS magnet which is a solenoid comprised of niobium-titanium coils capable of producing a 4 T magnetic field. For the purposes of longevity to the CMS magnet is currently running at 3.8 T instead of its full strength of 4 T. The magnet is the key instrument of the detector as it allows for the measurement of path curvature from which one can derive the momentum of the particles produced.

4.0.5 Muon Detectors

The last layer of the CMS detector includes the muon chambers. Muons can easily pass through all the previous layers of highly dense material while most other particles will be absorbed. As such, the most likely particle to be measured in this region are muons. Muons are measured at four muon stations which are spaced by the layers of highly dense iron "return yoke." These layers of highly dense iron help absorb any particles that should have been absorbed previous to the muon chambers.

4.0.6 Triggers

The LHC produces billions of collisions per second resulting in an unfathomable amount of data that is impossible to examine in entirety. In order to filter through the data, CMS uses triggers to remove events that are not considered interesting. This is done in two stages using the Level 1 Trigger (L1) and High Level Trigger (HLT). The L1 trigger searches for events that are more likely to contain new physics such as high energy events or an unusual combination of particles formed resulting from the collision.

These events are then sent to a server where the HLT will then select from candidate events chosen by the L1 trigger, and reconstruct events to determine if they are interesting or not.

The L1 trigger for di-photon events triggers on events who contain two photons whose $P_T > 19$ GeV [2]. This analysis requires that there are at least two photons whose P_T is greater than 40 GeV, this allows access to the di-photon trigger ensuring that no data is lost in the L1 stage.

4.0.7 Smearing

From the CATFISH Monte-Carlo generated events, the S_T distribution was formed using all the information available from a collision including the information relating to invisible particles that would escape detection at CMS such as neutrinos and gravitons. As this is too far removed from real analysis the S_T distribution was produced using the vector imbalance which only requires the four vectors of each visible particle and the MET. As the imbalanced S_T only calculates the S_T based on measurable quantities, it is more similar to a real measurement than the idealized S_T is. However, even the imbalanced S_T is too idealized for real analysis; thus, we introduce a process known as smearing where uncertainty is added to the generated four vectors of each particle according to a Gaussian distribution that is weighted by the resolution of the CMS ECAL and HCAL defined previously.

Applying this smearing to the ideal S_T from the Monte-Carlo generates the plot shown below in Figure 4.2:

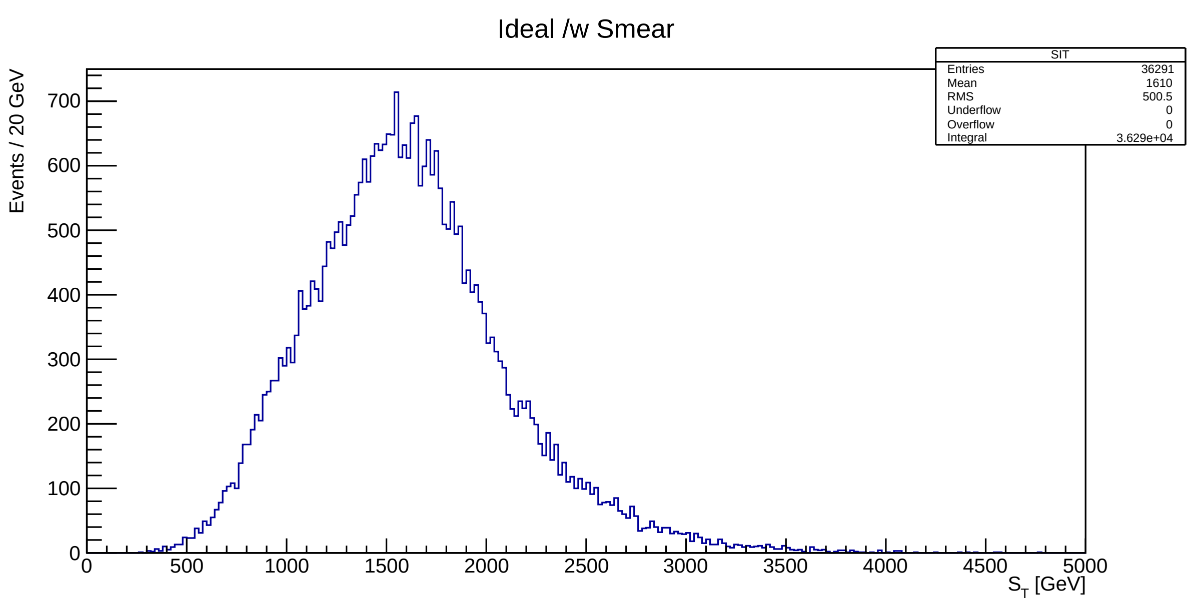

Figure 4.2: Ideal S_T Distribution from CATFISH Smeared to CMS Resolution

This S_T distribution is broader than the one produced from the Monte-Carlo generator CATFISH and provides a more complete image of how black hole production would manifest itself in the detector.

Plotting the the non-smeared $S_T$versus the smeared S_T illustrates this effect and is shown in Figure 4.3:

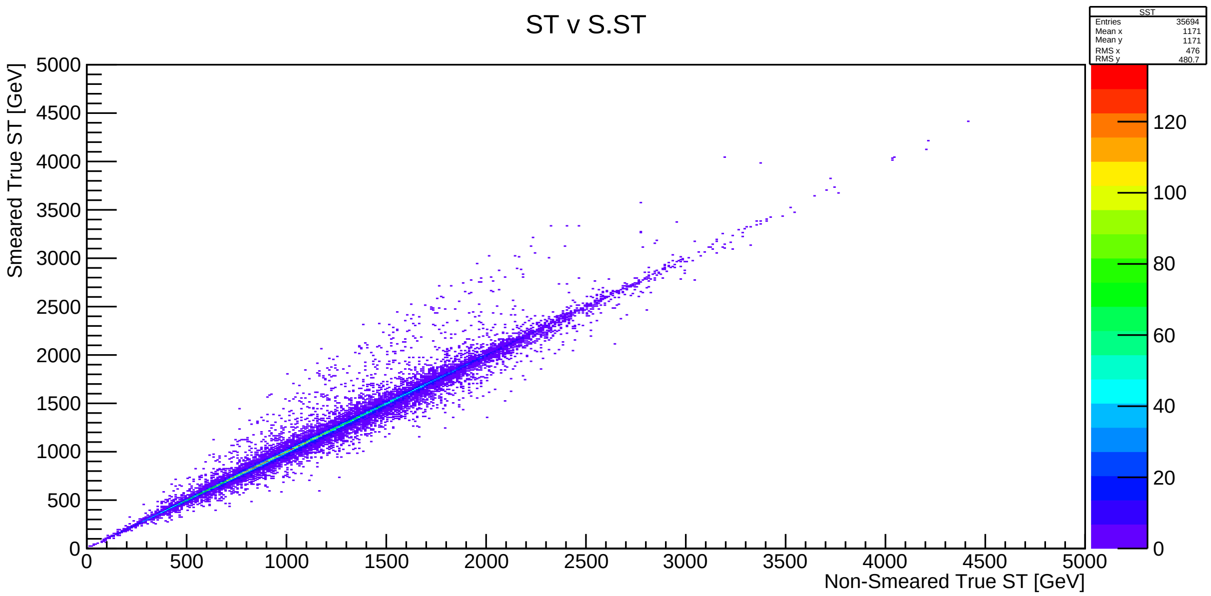

Figure 4.3: Ideal S_T Versus Smeared Ideal S_T

To provide a more a complete picture of what the S_T distribution would look like in the CMS detector, the same smearing process to the vector S_T distribution as shown in Figure 4.4.

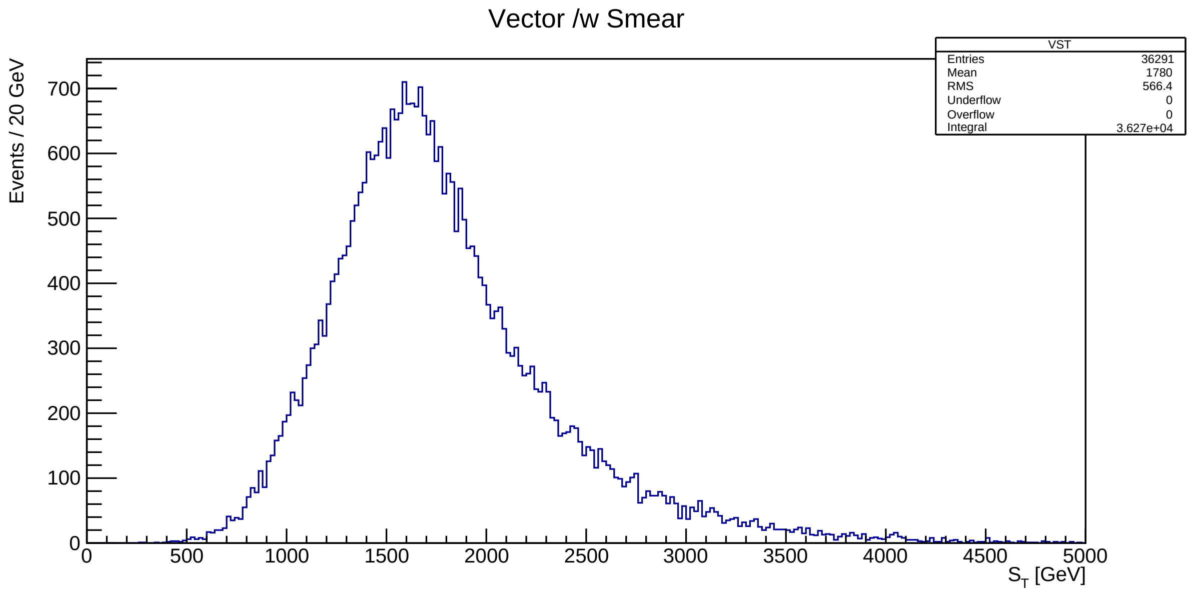

Figure 4.4: Vector Imbalance S_T Distribution from CATFISH Smeared to CMS Resolution

Just as before, to see how much smearing has broadened our S_T distribution a 2D plot is formed as shown in Figure 4.5

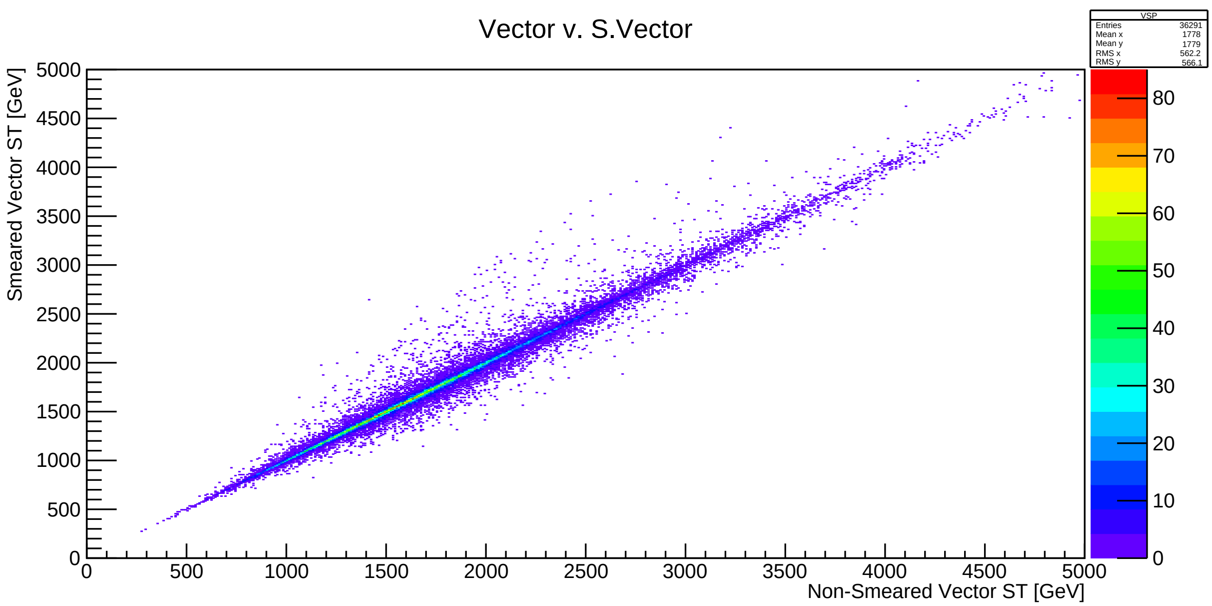

Figure 4.5: Vector Imbalance S_T versus Smeared Vector Imbalance S_T

An example of this smearing effect is shown in the plot below comparing the P_T of a smeared and non-smeared photon.

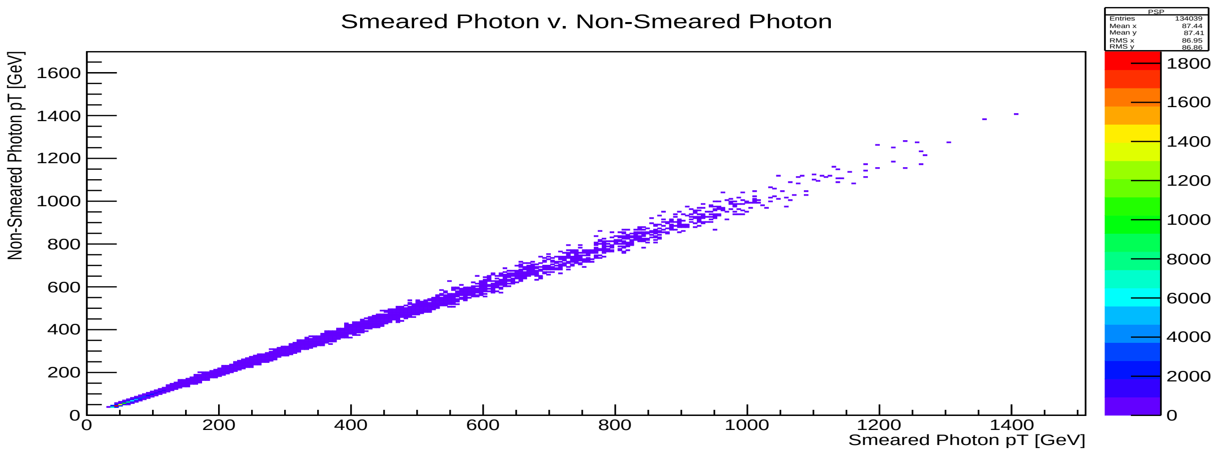

Figure 4.6: Smeared Photon P_T Versus Non-Smeared Photon P_T

This plot shows the effect of smearing according the ECAL resolution. Smearing successfully broadens the P_T values of the Photon generated from the Monte-Carlo to more closely resemble what CMS would measure.

One also wants to consider the how the HCAL smears particles. The following plot shows the effect of smearing on pions according to the HCAL resolution.

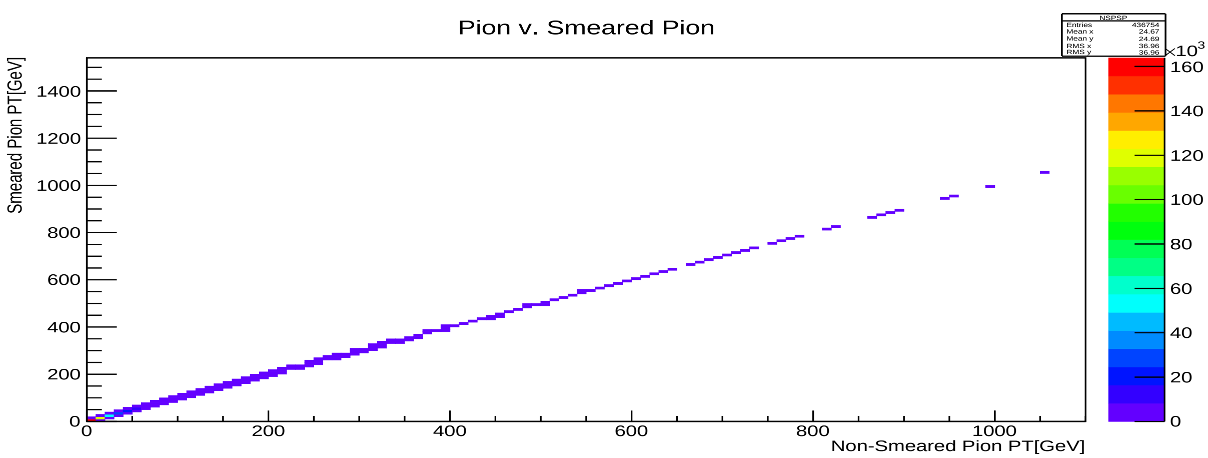

Figure 4.7: Smeared Pion P_T Versus Non-Smeared Pion P_T

This analysis also wants to consider how the the shape of the smeared vector S_T distribution changes as we require two photons versus zero photons.

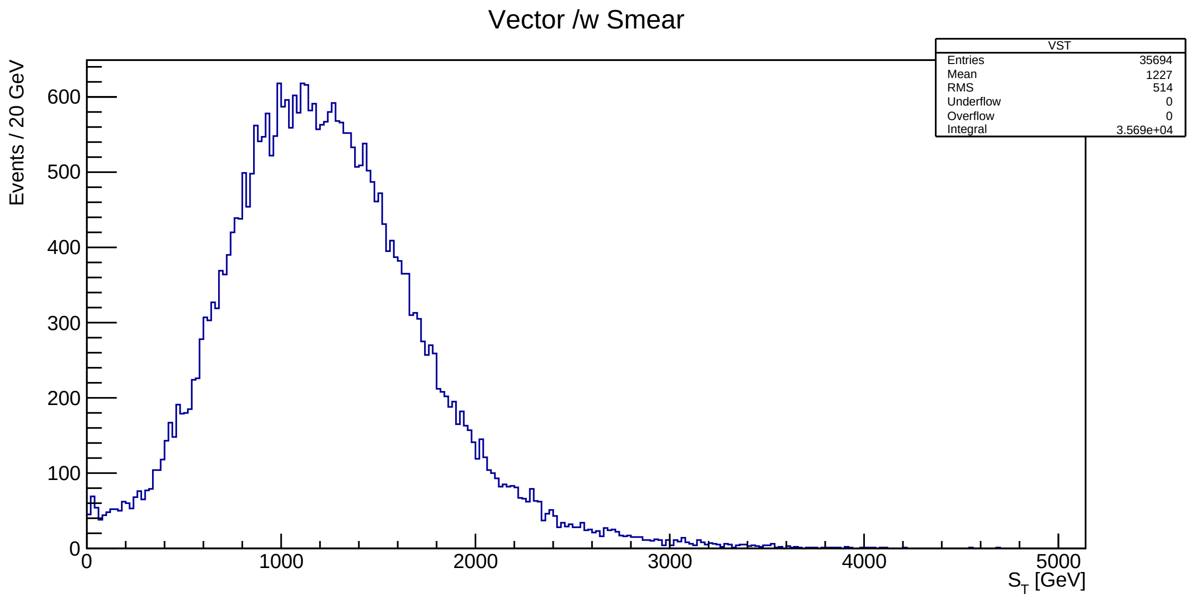

Figure 4.8: Smeared Vector ST for Events With Zero High Energy Photons

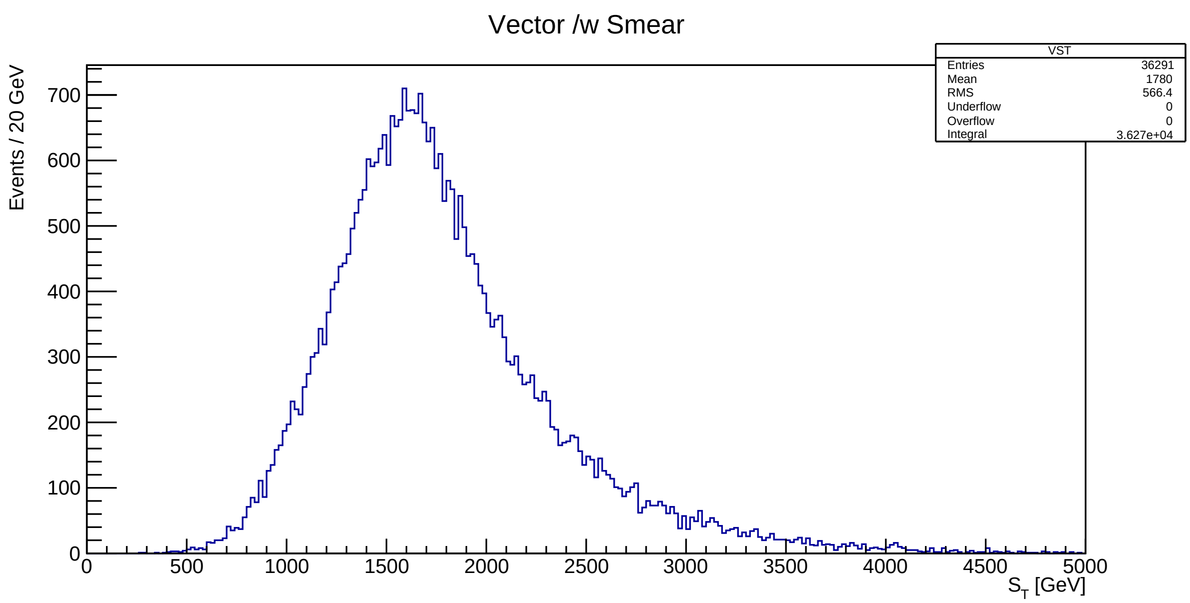

Figure 4.9: Smeared Vector S_T for Two+ Photon Events

From Figure 4.8 and Figure 4.9 one can see a clear distinction between the shape of the S_T distribution when requiring two or more photons whose $P_T > 40$ GeV versus the S_T distribution including everything else. The plot that excludes the high energy photons, Figure 4.8, has a much broader peak than the S_T distribution that includes the photons, Figure 4.9. One can also see that by these plots that photons are a large portion of the S_T spectrum as explicitly removing them shifts the peak into a much lower S_T region.

CHAPTER 5

DATA

5.0.1 LHC Data Information

This analysis will examine data obtained from the Run II at the LHC prior to August 2016 at center-of-mass energy $\sqrt{s}$=13 TeV with an integrated luminosity of 12.9 $\pm$0.8 fb^{-1}. This will be the first thesis to analyze this data for microscopic black hole production under the condition of two photons in the final state.

5.0.2 Method of Analysis

The microscopic black holes will decay to all SM particles via Hawking radiation. The transverse momenta resulting from the collision is a sizable fraction of the beams energy [10] making the sum of transverse momenta (S_T), a well-defined measurable distribution that can be used in a search for quantum black holes.

Without the production of black holes the S_T distribution is expected to be a falling exponential dominated by QCD. What one expects to see in the case of black hole production is that at some P_T threshold black holes begin to form resulting in some structure formation in the S_T distribution that would not be present otherwise.

As black hole production results in a "broad excess in the S_T spectrum rather than a narrow peak" one is unable to use current methods of analysis to model the multi-jet background in the signal region where black holes are produced. During Run I of the LHC however, a new method of analysis was used showing that the shape of the S_T distribution remains the same regardless of the number of objects in the final state. Thus, one can use a low multiplicity control region to predict the shape of the S_T distribution in multi-jet events. This method is known as S_T Scaling and is a powerful tool in searching for new physics.

This analysis differs from the previous black hole searches at CMS due to the requirement of two photons. By this requirement one can gain access to the diphoton trigger allowing this analysis to access an unexplored region of phase space that is high in S_T.

CHAPTER 6

SELECTION

One of the unique characteristics of this analysis is the requirement that there exist two high P_T photons in an event to be considered a candidate. No previous search for quantum black hole production has discriminated on the type of particles required in the final state. In order to ensure that these particles are indeed photons, the following selection cuts are introduced that remove a significant portion of background and noise.

6.0.1 Photon Multiplicity Cut

This analysis requires at least two photons whose $P_T > 40$ GeV. Plotting the leading and trailing photon P_T produces figures 6.1 and 6.2 respectively.

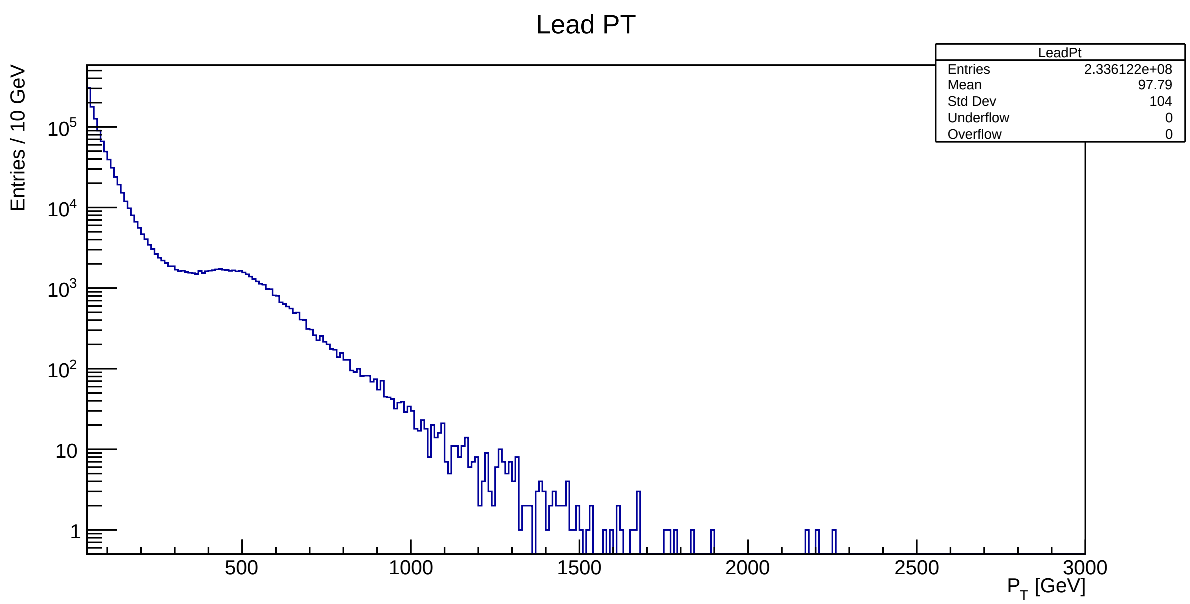

Figure 6.1: Leading Photon PT

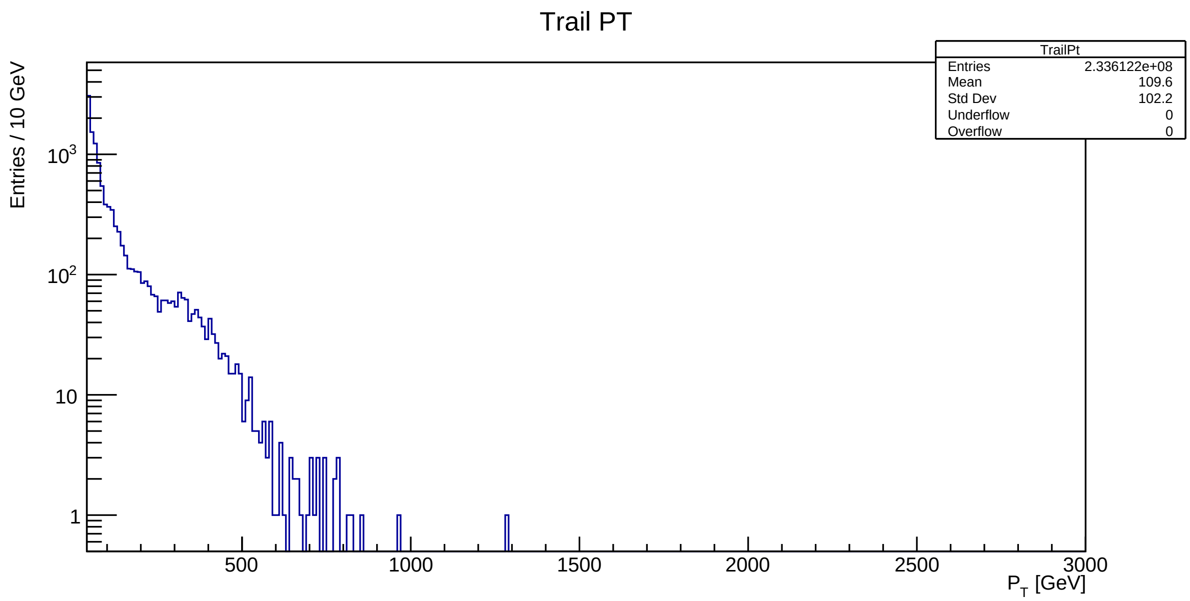

Figure 6.2: Trailing Photon PT

6.0.2 Calorimeter Region Selection Cuts

This analysis also requires that these photons are in the barrel of the calorimeter defined as the region $|\eta| < 1.4$. The reasoning behind only accepting particles in the barrel is that those particles can be reconstructed with a higher resolution than particles found in the end cap. Figure 6.3 shows the distribution of photons within the barrel of the calorimeter in η and Figure 6.4 shows the distribution in phi.

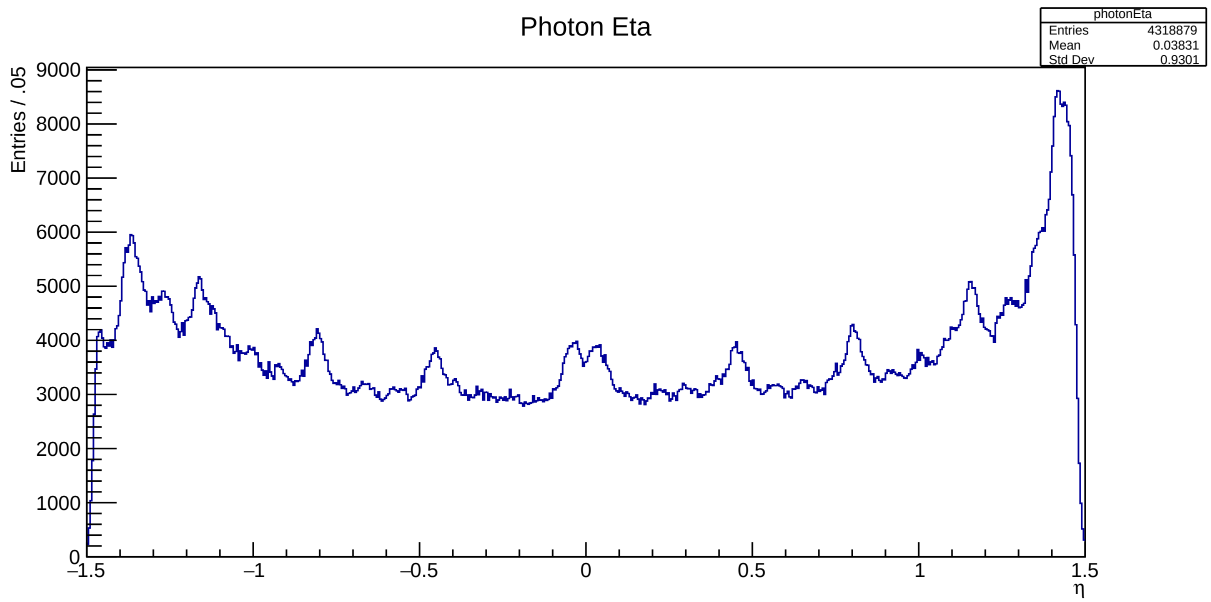

Figure 6.3: Photon Eta

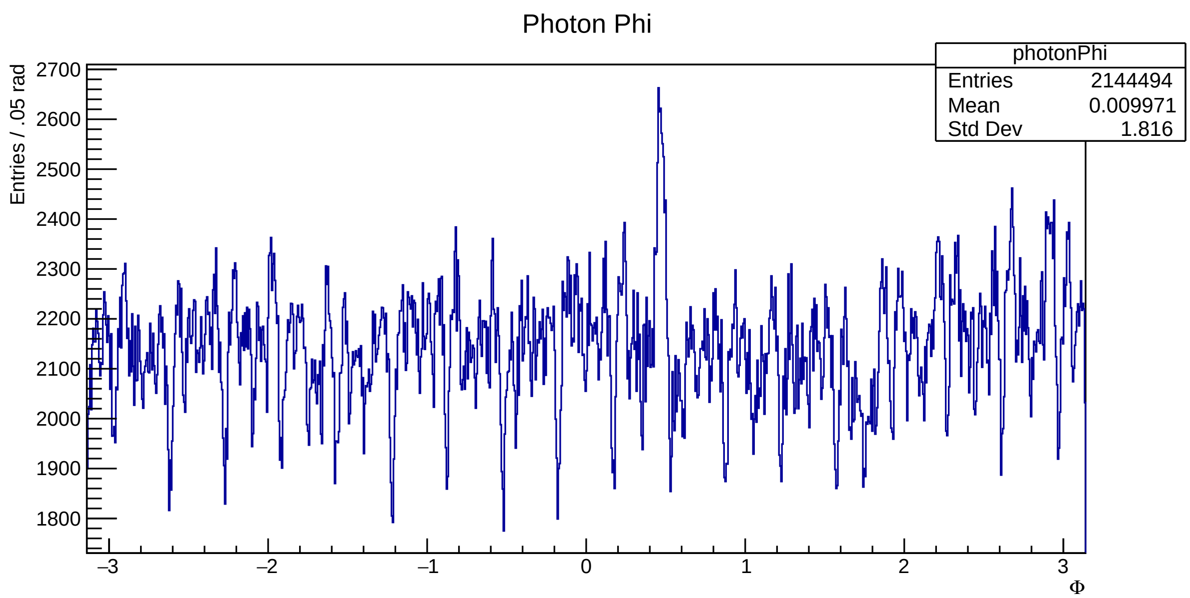

Figure 6.4: Photon Phi

6.0.3 Photon Identification Cuts

To ensure our object is indeed a photon, this analysis requires the ratio of the energy deposited in the hadronic calorimeter to that deposited in the electromagnetic calorimeter defined as $\frac{H}{E}$ to be:

$$\frac{H}{E} < 0.05 \tag{6.1}$$

To further ensure that our objects are indeed photons this analysis considers the quantity $\sigma_{i\eta i\eta}$ which is defined as the shower width and is calculated as follows:

$$\sigma^2_{i\eta i\eta} = \frac{\sum_{5x5} w_i(\bar{\eta} - \eta_i)^2}{\sum_{5x5} w_i} \tag{6.2}$$

This equation is a sum over all 5x5 crystals where w_i is a logarithmic weight on the crystal with index i, $\bar{\eta}$ is the energy weighted average η for a shower, and η_i is the position in eta of the crystal with index i [4]. The weighting w_i is defined as:

$$w_i = max(0, w_0 + ln(\frac{E_i}{E_{5x5}})) \tag{6.3}$$

Where w_0 is an optimized free parameter, E_i is the energy deposited in the crystal with index i and E_{5x5} represents the total energy deposted in a 5x5 grid of crystals. This is quantity is related to the variance about the mean in η and helps discriminate against jets. It does this by using the fact that hadronic jets are composed of many objects, and as such they will manifest themselves in the detector with a wider shower width than that of photons. Thus, this analysis requires $\sigma_{i\eta i\eta} <.0102$ for the photon to be accepted as a candidate. The $\sigma_{i\eta i\eta}$ distribution is shown in Fig. 6.5.

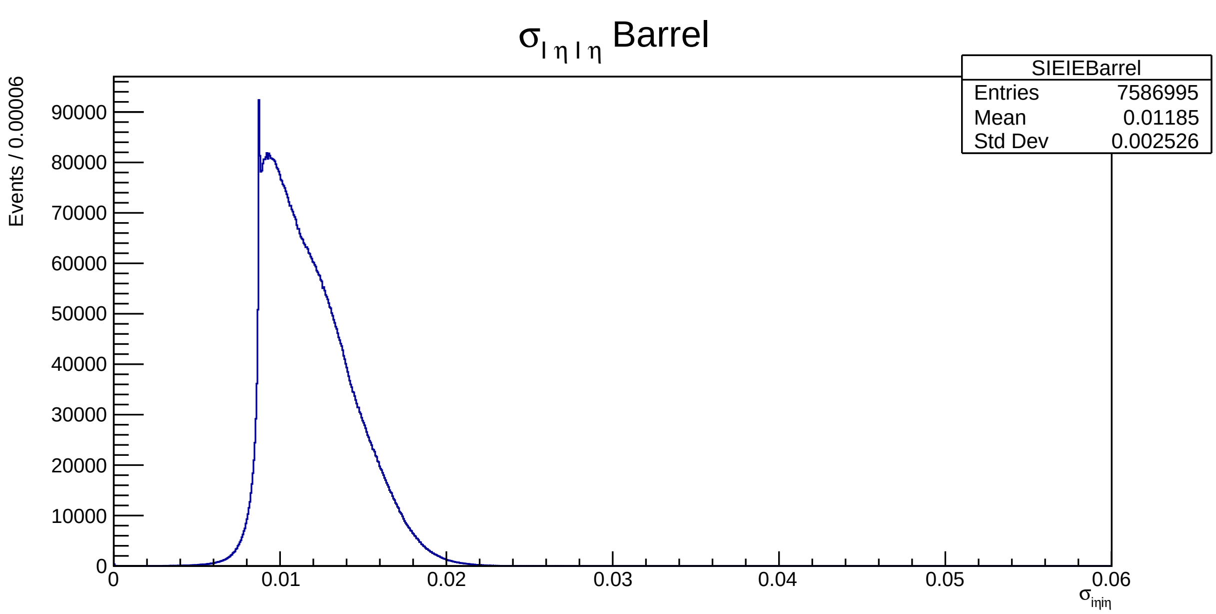

Figure 6.5: $\sigma_{i\eta i\eta}$ Distribution

Isolation is introduced to reduce the number of objects mimicking a real photon by requiring there to be no high-energy objects near the selected particle.

Table 6.1: Isolation Requirements

Barrel	Loose(90.4%)	Medium (79.9%)	Tight (70.1%)
Background Rejection	Loose (83.8%)	Medium (86.9%)	Tight (88.9%)
HoverE	0.05	0.05	0.05
$\sigma_{i\eta i\eta}$	0.0102	0.0102	0.0100
PF Charged Hadron Isolation	3.32	1.37	.76
PF Neutral Hadron Isolation	1.92+0.014*$P_{T,\gamma}$+0.000019*$P_{T,\gamma}^2$	1.06+0.014*$P_{T,\gamma}$+0.000019*$P_{T,\gamma}^2$	0.97+0.014*$P_{T,\gamma}$+0.000019*$P_{T,\gamma}^2$
PF Photon Isolation	.81+0.0053*$P_{T,\gamma}$	.28+0.0053*$P_{T,\gamma}$	.08+0.0053*$P_{T,\gamma}$

This analysis will use the medium isolation requirements as that set of cuts removes a significant portion of background without removing too many events from the signal region. The medium isolation requirements are also chosen for their use in previous black hole searches at CMS.

CHAPTER 7

ANALYSIS

After the event is considered a candidate by passing all selection requirements, the S_T distribution is formed by taking the scalar sum of momentum in the transverse direction of photons, leptons, jets and MET for each event. This produces Fig. 7.1.

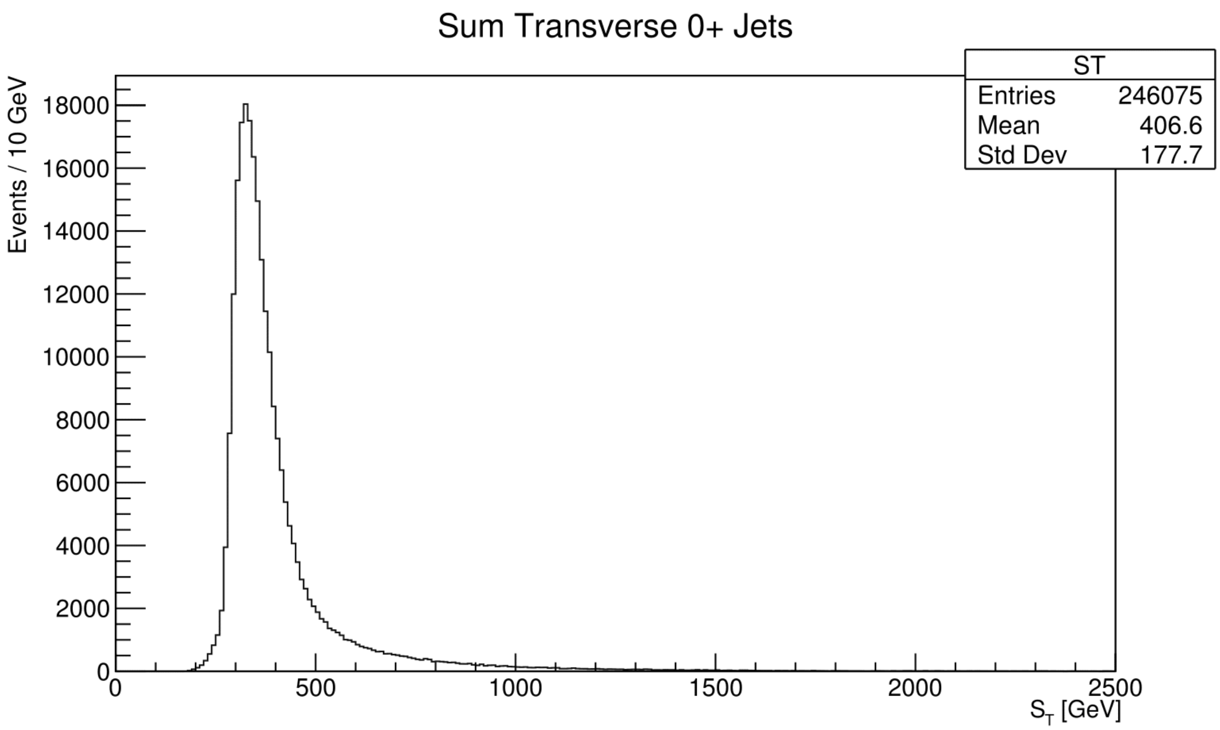

Figure 7.1: 0+ Jet S_T For Two Good Photons

As the shape of S_T distribution for QCD does not change with object multiplicity, one is able to generate the background for these events using S_T scaling. This is done by fitting the S_T distribution for low jet multiplicity events to a functional form.

7.0.1 Functional Form

The S_T distribution is fit to the following functional form:

$$f(x) = \frac{P_0(1+x)^{P_1}}{x^{P_2+P_3\log(x)}} \tag{7.1}$$

Fitting determines the values of P_N for the functional form defined for each jet multiplicity requirement.

This allows for the creation of curves that estimate our background shape. The Monte-Carlo generator CATFISH has shown that events with a low jet multiplicity are unlikely to contain black hole production and as such are safe to use as a control region to form backgrounds from.

Doing so produces the following table of values for events requiring two good photons shown in table 7.1.

Table 7.1: P_N Values for Two Good Photons

Parameter	Zero Jets	One Jet	Two Jet
P_0	.01897 $\pm$ .00832	1.376 $\pm$ .462	9.503 $\pm$ 1.793
P_1	6.836 $\pm$ .118	7 $\pm$ .1	3.086 $\pm$ .328
P_2	.05611 $\pm$ .00746	2.576 $\pm$ .139	.2332 $\pm$ .2046
P_3	0.8025 $\pm$ .0098	.5625 $\pm$ .0086	.0475 $\pm$ 0.0154

In order to compare each functional form $f_J(x)$ one must apply integral normalization as defined in the following equation.

$$C_j \int_{600}^{700} f_j(x)dx = 1 \tag{7.2}$$

Where j refers to the explicit number of jets required and C_j is some normalization constant. Plotting the normalized functional forms produce the following envelope plot for two good photons:

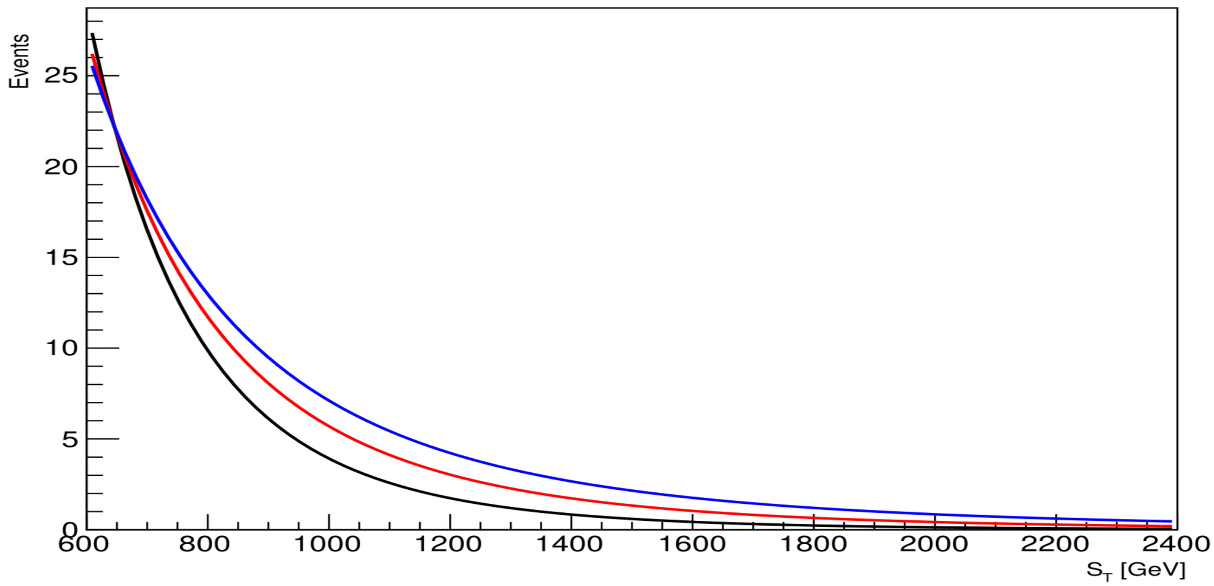

Figure 7.2: Integral Normalized $f(x)$ For 2 Good Photons and Varied Jet Multiplicity

In 7.2 The black curve represents $f_0(x)$, the red curve represents $f_1(x)$, and the blue curve represents $f_2(x)$.

In order to increase the number of statistics available this analysis would also want to consider the case of only one photon passing all selection requirements and one photon that does not. Doing so produces the following P_N values:

Table 7.2: P_N Values for One Good and 1 Bad Photon

Parameter	Zero Jets	One Jet	Two Jet
P_0	3.121 ± 0.159	$.6461 \pm .0653$	$1.001 \pm .524$
P_1	$6.722 \pm .016$	$5.863 \pm .029$	$6.256 \pm .119$
P_2	$.2177 \pm 0.0016$	$.02508 \pm .00091$	1.6 ± 0.0
P_3	$.7969 \pm 0.0012$	$0.6881 \pm .0023$	$.5912 \pm 0.0104$

Applying the same integral normalization technique referenced earlier, the following envelope plot is produced by requiring only one photon to pass all selection requirements and one photon that does not.

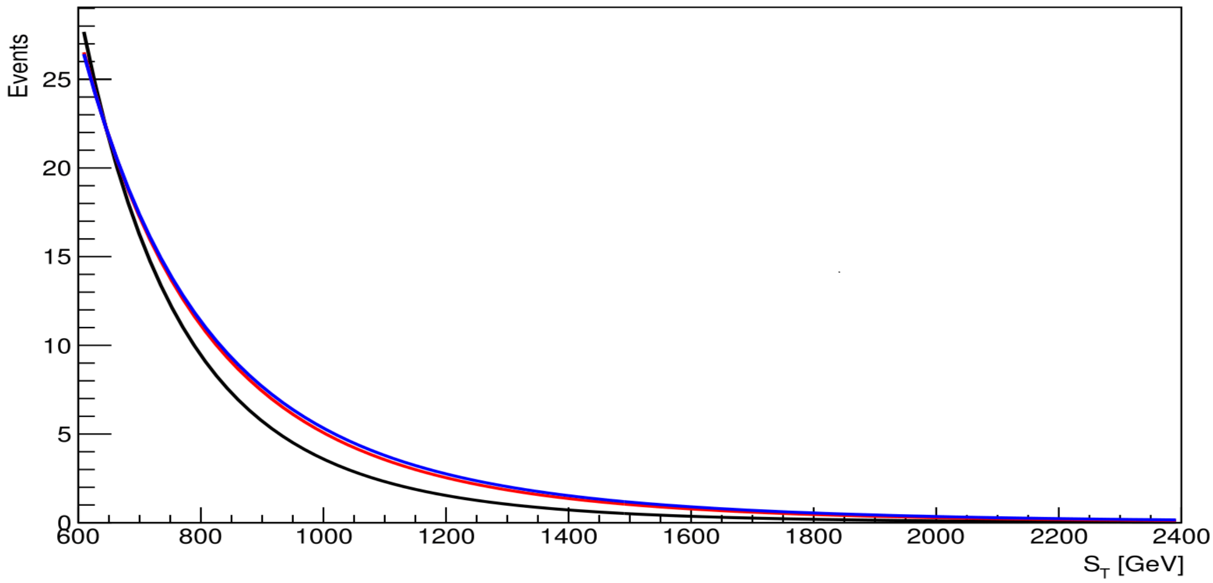

Figure 7.3: Integral Normalized $f(x)$ For 1 Good Photon 1 Bad Photon and Varied Jet Multiplicity

In 7.3 The black curve represents $f_0(x)$, the red curve represents $f_1(x)$, and the blue curve represents $f_2(x)$.

7.0.2 Control Region Fit on Signal Region

The control region in which this analysis can safely say there would be almost no black hole production, as shown in the Monte-Carlo generator CATFISH, is the black curve which contains zero jets. As the number of jets increases, so does the risk that the background will be contaminated by signal.

Scaling the integral normalized curves onto the the S_T distribution for 3+ Jets will determine if there is a significant excess of events produced that is not indicative of QCD.

For the case of two good photons, scaling the integral normalized curves onto the 3+ jet S_T distribution forms Figure 7.4

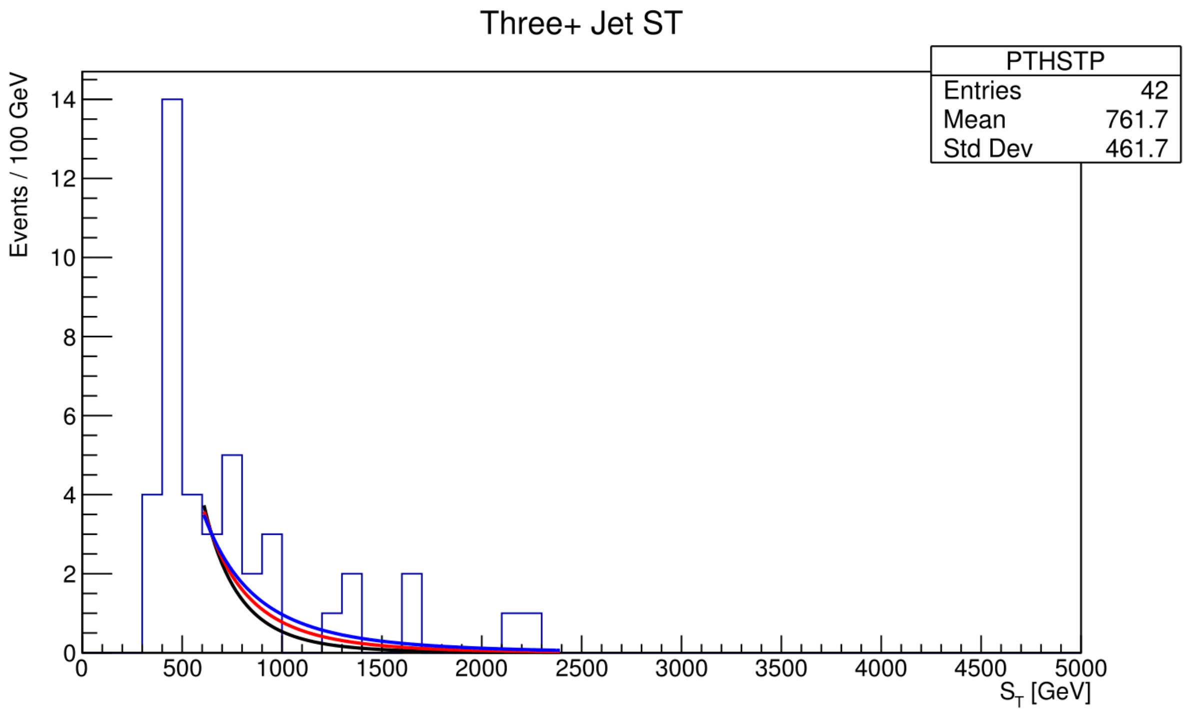

Figure 7.4: 0,1,2 Jets $f(x)$ For 2 Good Photons Scaled to 3+ Jet S_T

In figure 7.4 the black curve represents $f_0(x)$, the red curve represents the 1 jet $f_1(x)$ and the blue curve represents the 2 jet $f_2(x)$. Examining explicitly over the signal region yields the following plot seen in Fig. 7.5.

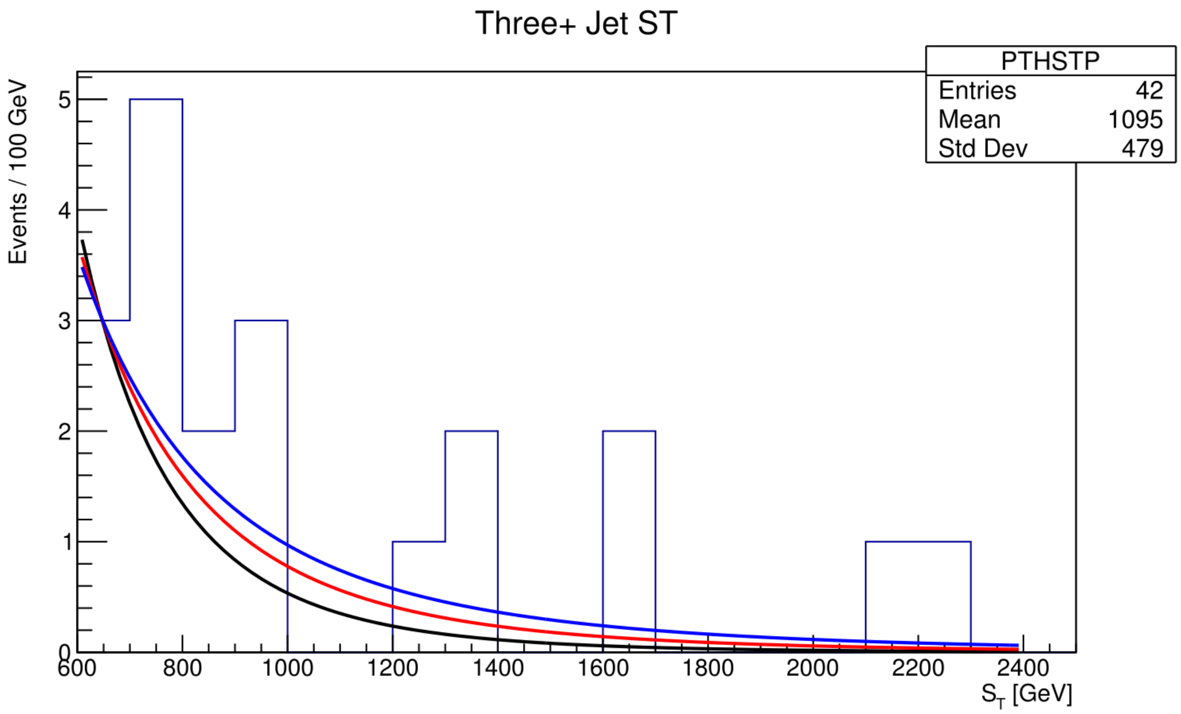

Figure 7.5: 0,1,2 Jets $f(x)$ For 2 Good Photons Scaled to 3+ Jet Signal Region S_T

The integral of bins in data in the region 1500 to 2400 GeV is the number of events measured in data for 2 good photons corresponding to the expected signal region generated from the Monte-Carlo and is equal to 4 events. Integrating the curves over the range above yields the following values for what is expected from QCD.

Table 7.3: Integral of $f_j(x)$ from 1500 to 2400 for 2 Good Photons

$f_j(x)$	Integral of $f_j(x)$
$f_0(x)$	1.5
$f_1(x)$	3.6
$f_2(x)$	4.3

Now the same scaling is applied to the integral normalized curves generated from events that contain one good photon and one bad photon. Doing so produces the following plot shown in Fig. 7.6:

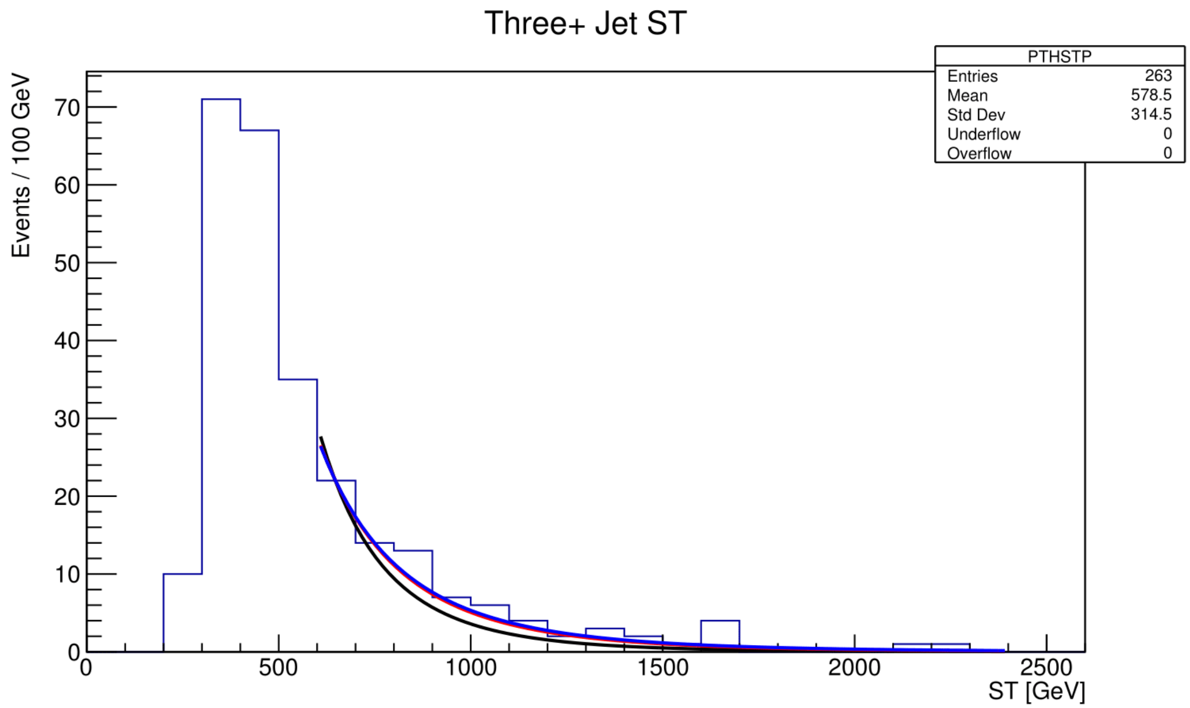

Figure 7.6: 0,1,2 Jets $f(x)$ For 1 Good Photon 1 Bad Photon Scaled to 3+ Jet S_T

In Figure 7.6 the black curve represents $f_0(x)$, the red curve represents the 1 jet $f_1(x)$ and the blue curve represents the 2 jet $f_2(x)$.

Closer examination over the signal region yields Figure 7.7.

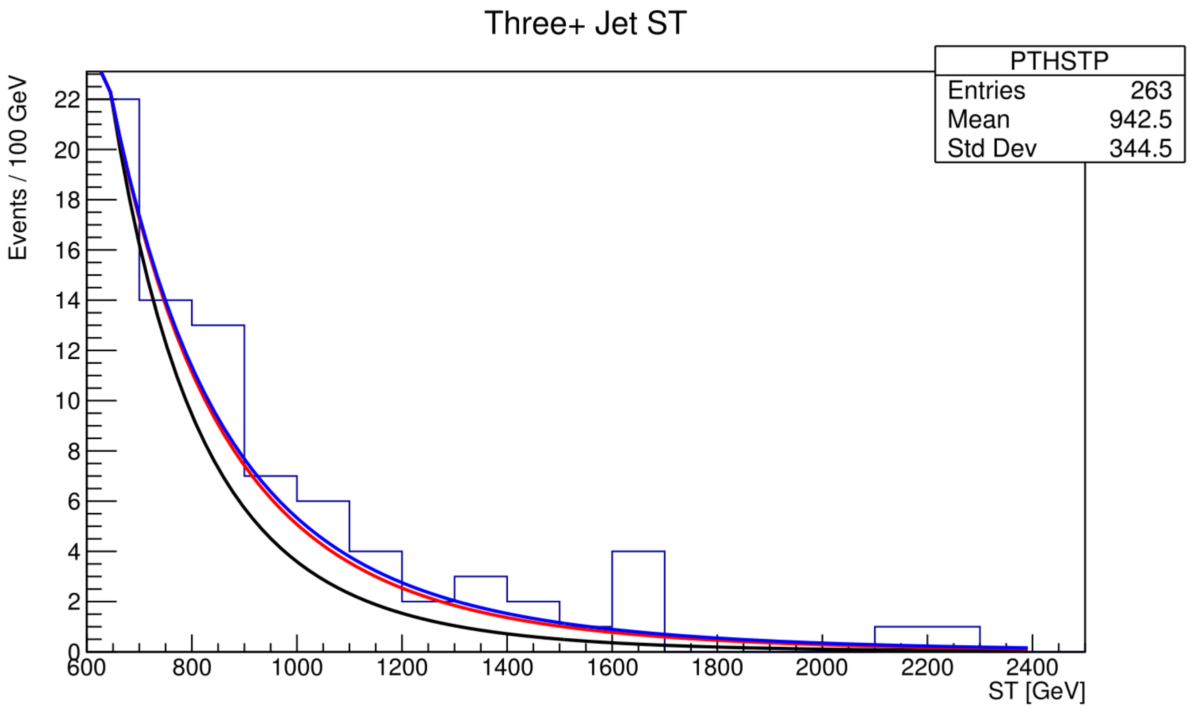

Figure 7.7: 0 Jet $f(x)$ For 1 Good Photon 1 Bad Photon Scaled to 3+ Jet Signal Region S_T

The integral of bins in data in the region 1500 to 2400 GeV is the number of events measured in data for 1 good / 1 bad photon and is equal to 7 events. Integrating the curves over the range above yields the following values for what is expected from QCD.

Table 7.4: Integral of $f_j(x)$ from 1500 to 2400 for 1 Good 1 Bad Photon

$f_j(x)$	Integral of $f_j(x)$
$f_0(x)$	1.8
$f_1(x)$	5.1
$f_2(x)$	9.4

CHAPTER 8

RESULTS

This analysis searched for quantum black hole production at $\sqrt{s}$= 13 TeV requiring two high E_T photons in the final state at the LHC. Using methods defined in previous searches at CMS this analysis concludes that there is no statistically significant excess in the signal region as the number of observed events falls within the range of values expected from QCD. Further studies can impose cross-section limits on the production of quantum black holes in this signal region.

BIBLIOGRAPHY

[1] Search for Black Holes with Early Run 2 Data. Technical Report CMS-PAS-EXO-15-007, CERN, Geneva, 2015.

[2] W. Adam et al. The CMS high level trigger. *Eur. Phys. J.*, C46:605–667, 2006.

[3] Nima Arkani-Hamed, Savas Dimopoulos, and G. R. Dvali. The Hierarchy problem and new dimensions at a millimeter. *Phys. Lett.*, B429:263–272, 1998.

[4] Andrew Askew. *Shower Width*, 2015.

[5] David Barney. *CMS Slice*, 2010.

[6] Marcus Bleicher, Piero Nicolini, Martin Sprenger, and Elizabeth Winstanley. Micro black holes in the laboratory. *Int. J. Mod. Phys.*, E20S2:7–14, 2011.

[7] Matteo Cacciari, Gavin P. Salam, and Gregory Soyez. FastJet User Manual. *Eur. Phys. J.*, C72:1896, 2012.

[8] M. Cavaglia, R. Godang, L. Cremaldi, and D. Summers. Catfish: A Monte Carlo simulator for black holes at the LHC. *Comput. Phys. Commun.*, 177:506–517, 2007.

[9] S. Chatrchyan et al. The CMS Experiment at the CERN LHC. *JINST*, 3:S08004, 2008.

[10] Steven B. Giddings and Scott D. Thomas. High-energy colliders as black hole factories: The End of short distance physics. *Phys. Rev.*, D65:056010, 2002.

[11] Douglas M. Gingrich. Comparison of black hole generators for the LHC. 2006.

[12] John H. Schwarz. Introduction to superstring theory. *NATO Sci. Ser. C*, 566:143–187, 2001.

[13] Torbjorn Sjostrand, Stephen Mrenna, and Peter Z. Skands. PYTHIA 6.4 Physics and Manual. *JHEP*, 05:026, 2006.